Electronic Supplementary Material (ESI) for Physical Chemistry Chemical Physics.

Supporting Information **for**

The regulatory function of d-orbital structure in TM@g-t-C_4N_3 for bifunctional catalysis of oxygen evolution/reduction reaction

Zhenduo Wang, Meichen Wu, Yuhong Huang, Jianmin Zhang *, Xiumei Wei *

School of Physics and Information Technology, Shaanxi Normal University, Xi'an, 710119, China

*Corresponding author. E-mail: weixiumei@snnu.edu.cn (X. Wei); jmzhang@snnu.edu.cn (J. Zhang).

Computational details for OER/ORR process

The reaction pathways of OER and ORR in acidic media are as follows:

The OER contains four elementary reaction steps:

$$* + H_2O(l) \rightarrow *OH + H^+ + e^- \quad \text{(S1)}$$

$$*OH \rightarrow *O + H^+ + e^- \quad \text{(S2)}$$

$$*O + H_2O(l) \rightarrow *OOH + H^+ + e^- \quad \text{(S3)}$$

$$*OOH \rightarrow * + O_2(g) + H^+ + e^- \quad \text{(S4)}$$

As the reverse reaction of OER, the ORR involves four inverse steps:

$$* + O_2(g) + H^+ + e^- \rightarrow *OOH \quad \text{(S5)}$$

$$*OOH + H^+ + e^- \rightarrow *O + H_2O(l) \quad \text{(S6)}$$

$$*O + H^+ + e^- \rightarrow *OH \quad \text{(S7)}$$

$$*OH + H^+ + e^- \rightarrow * + H_2O(l) \quad \text{(S8)}$$

The adsorption energies of reaction species (*OH, *O and *OOH) can be calculated by:

$$\Delta E_{*OH} = E_{*OH} - E_* - E_{OH} = E_{*OH} - E_* - (E_{H2O} - 1/2E_{H_2}) \quad \text{(S9)}$$

$$\Delta E_{*O} = E_{*O} - E_* - E_O = E_{*O} - E_* - (E_{H_2O} - E_{H_2}) \quad \text{(S10)}$$

$$\Delta E_{*OOH} = E_{*OOH} - E_* - E_{OOH} = E_{*OOH} - E_* - (2E_{H_2O} - 3/2E_{H_2}) \quad \text{(S11)}$$

where E_{H2O} and E_{H2} are the energies of H_2O and H_2 molecules in gas phase, respectively. According to previous work,[1] their adsorption Gibbs free energies can be approximated as:

$$\Delta G_{*OH} = \Delta E_{*OH} + 0.35\ eV \quad \text{(S12)}$$

$$\Delta G_{*O} = \Delta E_{*O} + 0.05\ eV \quad \text{(S13)}$$

$$\Delta G_{*OOH} = \Delta E_{*OOH} + 0.40\ eV \quad \text{(S14)}$$

Therefore, the reaction Gibbs free energies of steps (S1) - (S8) can be calculated by:

$$\Delta G_1 = \Delta G_{*OH} \quad \text{(S15)}$$

$$\Delta G_2 = \Delta G_{*O} - \Delta G_{*OH} \quad \text{(S16)}$$

$$\Delta G_3 = \Delta G_{*OOH} - \Delta G_{*O} \tag{S17}$$

$$\Delta G_4 = 4.92\ eV - \Delta G_{*OOH} \tag{S18}$$

$$\Delta G_5 = \Delta G_{*OOH} - 4.92\ eV \tag{S19}$$

$$\Delta G_6 = \Delta G_{*O} - \Delta G_{*OOH} \tag{S20}$$

$$\Delta G_7 = \Delta G_{*OH} - \Delta G_{*O} \tag{S21}$$

$$\Delta G_8 =- \Delta G_{*OH} \tag{S22}$$

Hence the theoretical overpotentials of OER and ORR can be expressed as:

$$\eta^{OER} = \frac{\max\{\Delta G_1,\ \Delta G_2, \Delta G_3, \Delta G_4\}}{e} - 1.23\ V \tag{S23}$$

$$\eta^{ORR} = \frac{\max\{\Delta G_5, \Delta G_6, \Delta G_7, \Delta G_8\}}{e} + 1.23\ V \tag{S24}$$

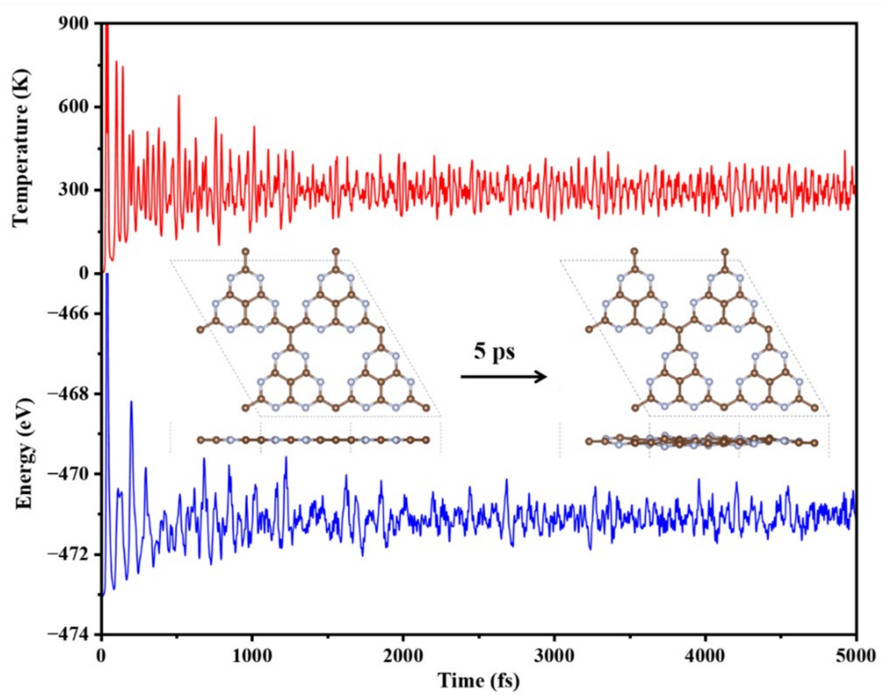

Fig. S1. The trends of temperature and total energy of g-t-C_4N_3 against time during the AIMD simulations at a temperature of 300 K. The insets show the top and side views of atomic structures of g-t-C_4N_3 before and after a 5-ps evolution.

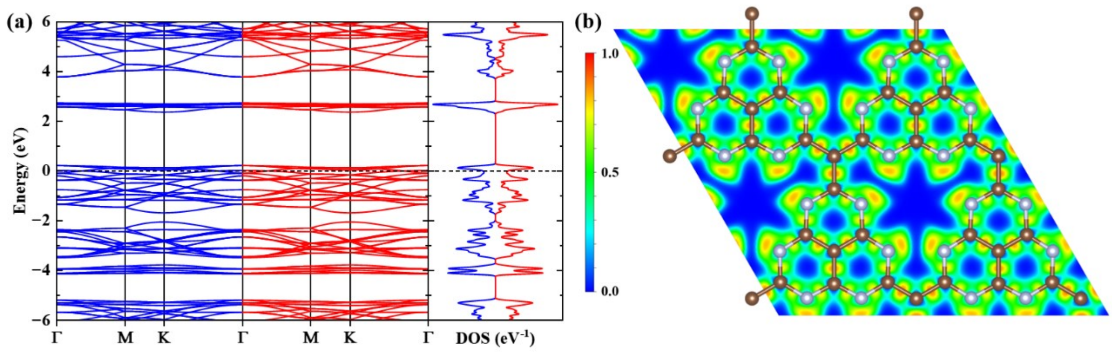

Fig. S2. (a) The spin-polarized band structure and DOS of g-t-C_4N_3. The spin-up and spin-down channels are marked in blue and red, respectively. The Fermi level is set to zero and plotted with black dashed line. **(b)** The ELF of g-t-C_4N_3. The color scale stands for the value of ELF.

Fig. S2(a) shows the spin-polarized band structure and DOS of pristine g-t-C_4N_3. It can be seen that the pristine slab exhibits nonmagnetic property due to the symmetric curves of spin-up and spin-down parts. Fig. S2(b) depicts the electron localization function (ELF) [2, 3] of g-t-C_4N_3. It is known that the ELF can be used to investigate the localized properties of electrons. To be specific, a value of zero (one) for ELF represents a fully non-localized (localized) state, while a value of 0.5 represents an electron-gas-like state. The six N atoms around the pore have relatively localized electrons, which implies that the TM@g-t-C_4N_3 might be stable when TM atoms are embedded in the pore.

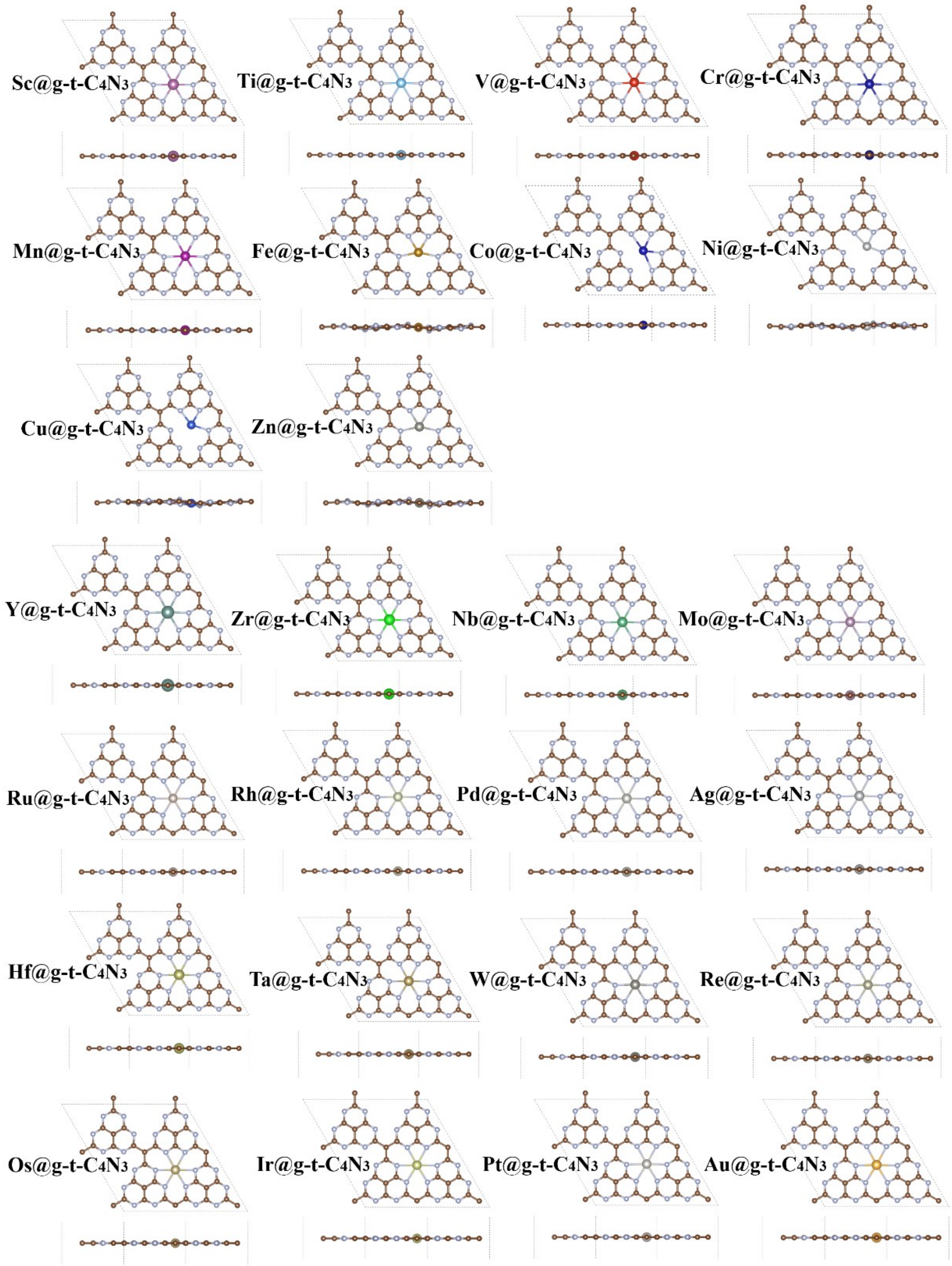

Fig. S3. Optimized structures of TM@g-t-C_4N_3. The brown and gray balls represent C and N atoms, respectively, and the balls with other colors represent corresponding TM atoms.

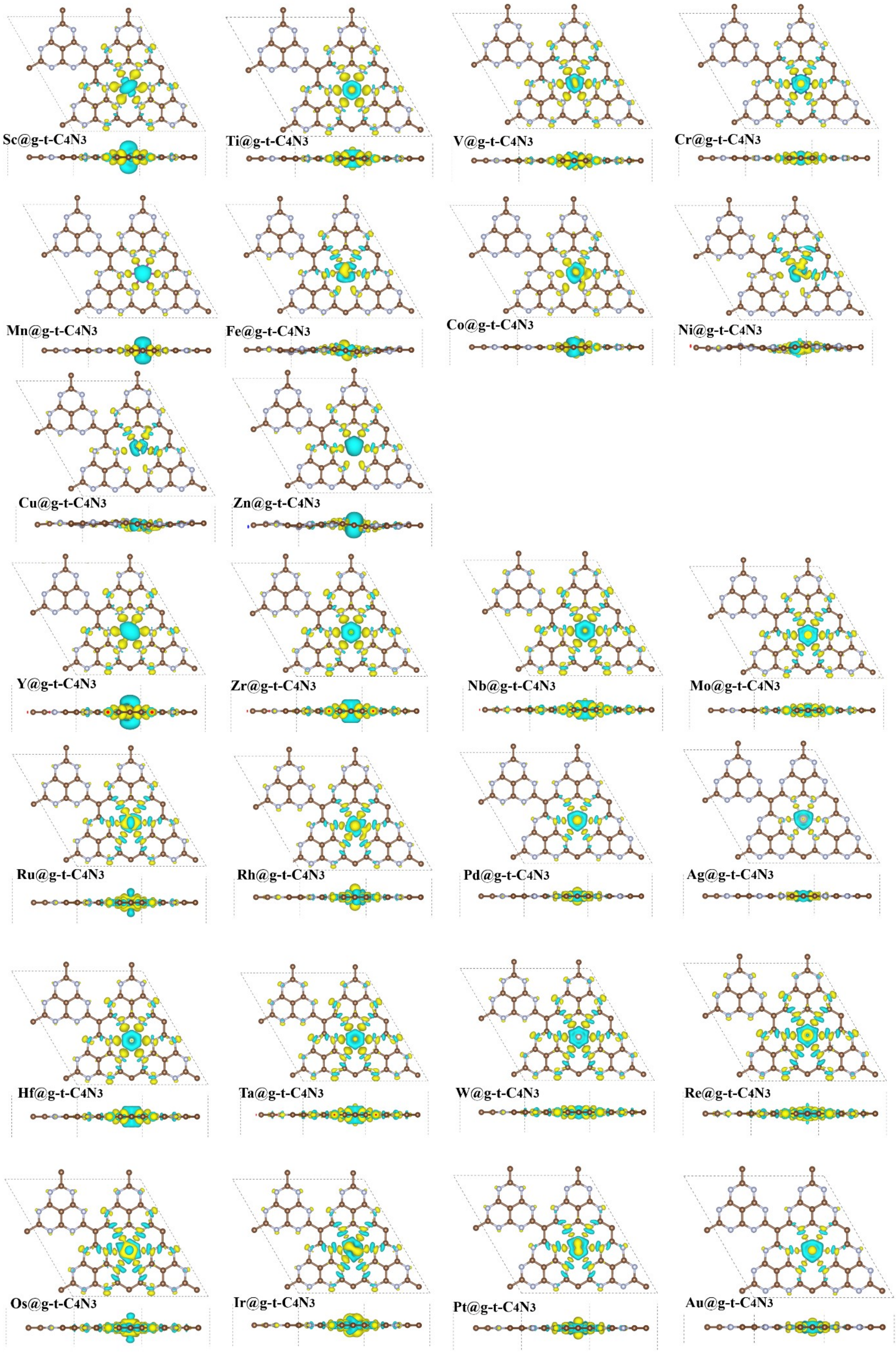

Fig. S4. The charge density difference of TM@g-t-C_4N_3. The yellow and cyan represent accumulation and depletion of electrons with the isovalue of 0.005 $e^-/bohr^3$.

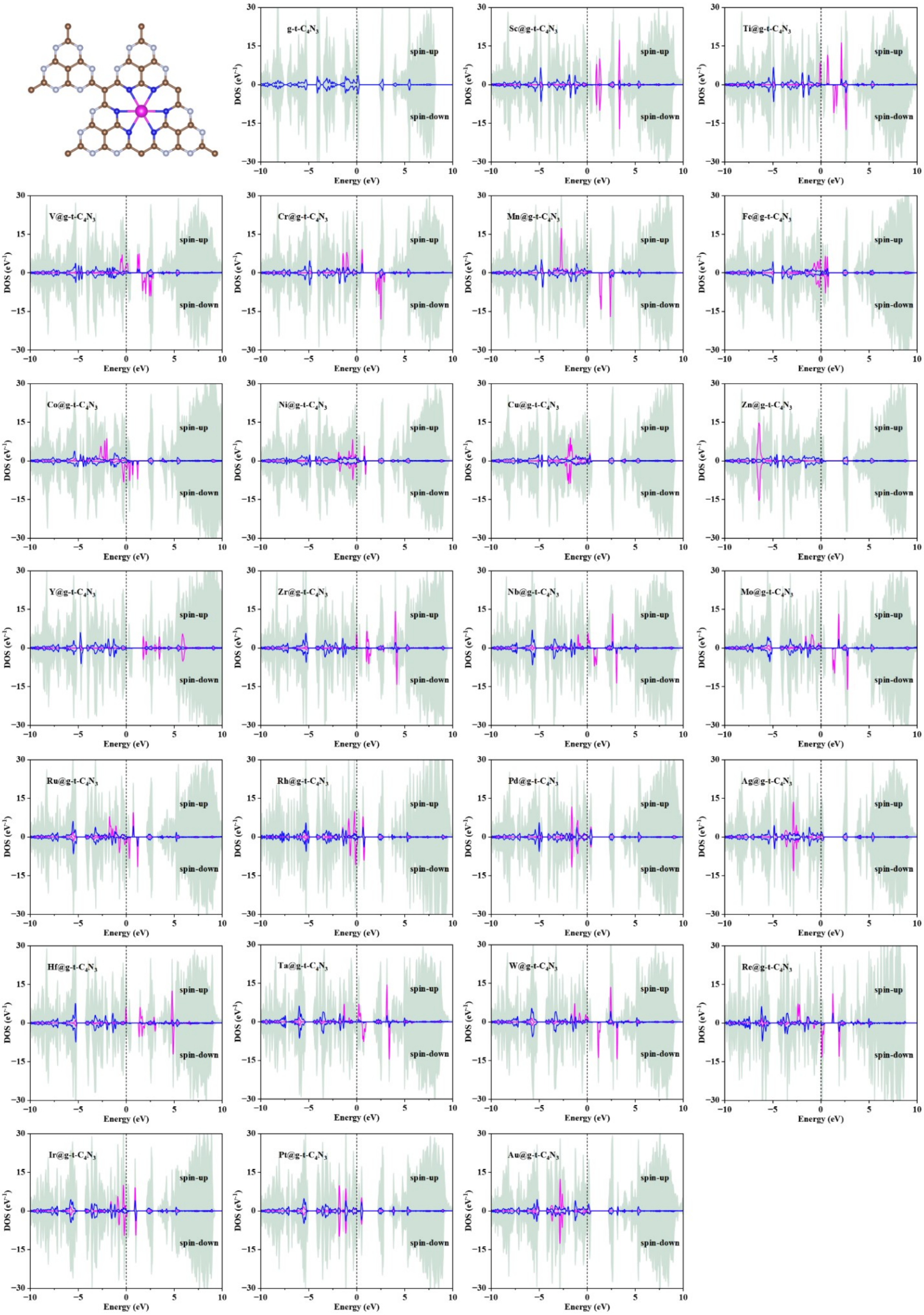

Fig. S5. The first subfigure shows the selected atoms (N atoms in blue and TM atom in magenta) in the structure of TM@g-t-C_4N_3. The others show the PDOS for corresponding structures with light-turquoise parts for total DOS, blue curves for p-states of selected N atoms and magenta curves for d-states of TM atom.

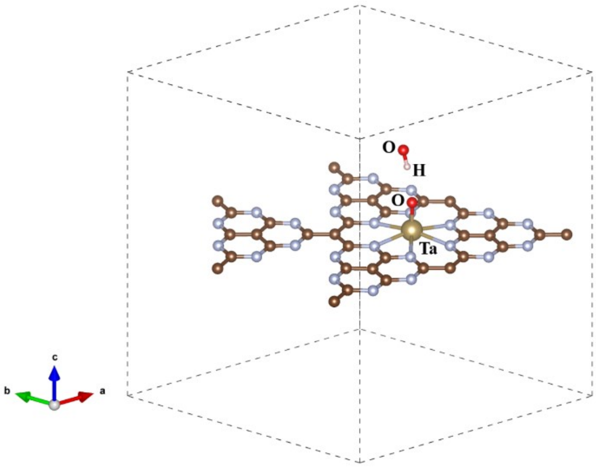

Fig. S6. The optimized structure of OOH group adsorbed on Ta@g-t-C_4N_3.

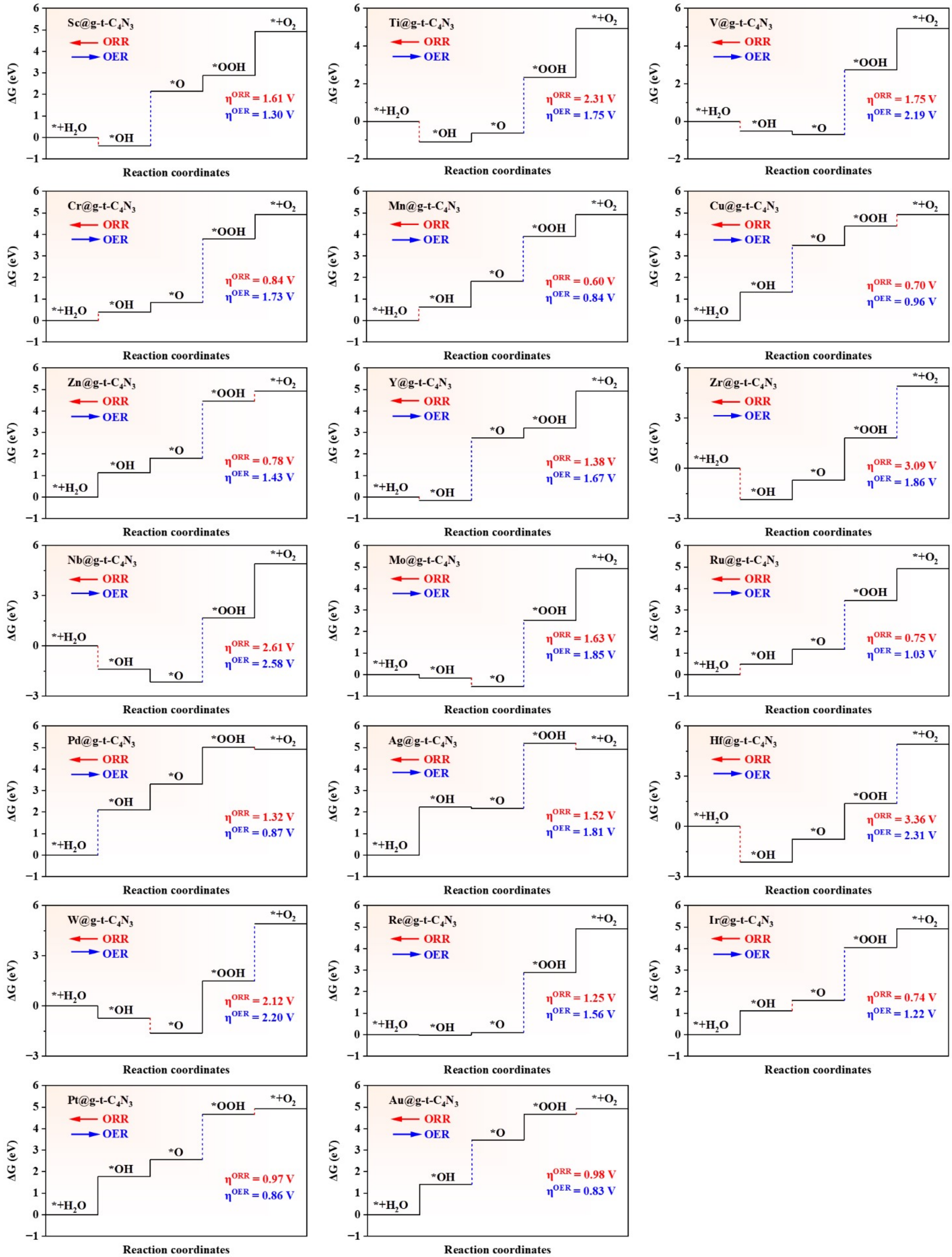

Fig. S7. The Gibbs free energy diagrams of TM@g-t-C_4N_3 for OER/ORR. The PDS is marked in blue/red dashed line for OER/ORR.

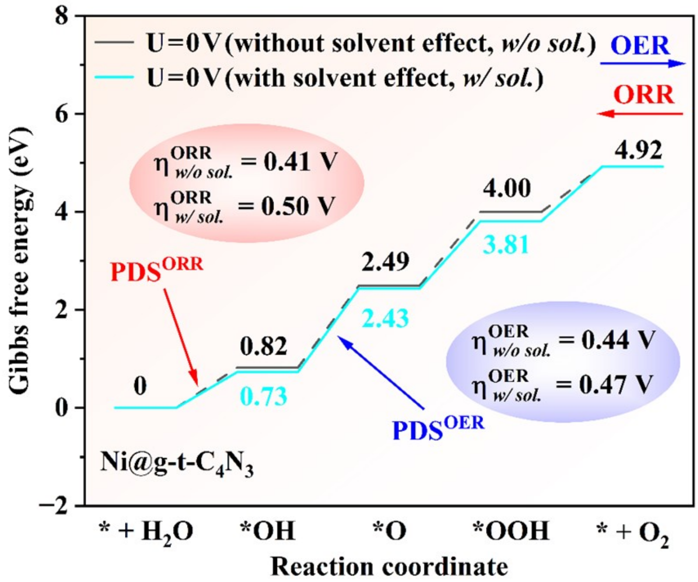

Fig. S8. The Gibbs free energy diagram of Ni@g-t-C_4N_3 before and after the consideration of solvent effects.

Taking the excellent Ni@g-t-C_4N_3 catalyst as an example, as shown in Fig. S8, both the Gibbs free energies and the overpotentials before and after the consideration of solvent effects are not significantly different. The overpotential difference of OER (ORR) with and without the consideration of solvent effects is only 0.03 V (0.09 V). It indicates that the solvent effects can be neglected for Ni@g-t-C_4N_3. Therefore, the solvent effects are not further considered in the work.

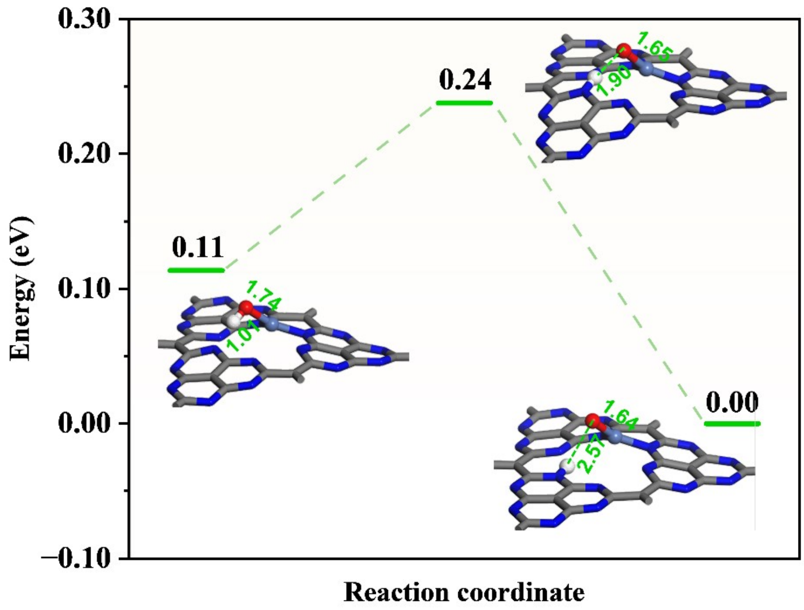

Fig. S9. The energy curve of transition states of *OH to *H-*O. The energy of *H-*O adsorbed on Ni@g-t-C_4N_3 is set to zero.

The Climbing Image-Nudged Elastic Band (CI-NEB) method was used to study the transition states and reaction kinetics.[4] Take the decomposition of *OH on the Ni@g-t-C_4N_3 as an example. The energy curve shows that the energy barrier from *OH to *H-*O on Ni@g-t-C_4N_3 is 0.13 eV, which is a relatively small barrier and means that the *OH intermediate on Ni@g-t-C_4N_3 is easy to decompose into *H-*O. However, the process shown here exhibited exothermic property which is different from that in the *OH to *O process. The main reason might be the structure of *H-*O is not the corresponding one (*O on the Ni@g-t-C_4N_3) involved in the OER process considered in this work. Therefore, we think that this approach might be a rough approximation for the investigation of transition states and reaction kinetics in the four-step OER mechanism. The transition states and the reaction kinetics of OER/ORR catalyzed by the g-t-C_4N_3 based SACs should be further investigated in a more detailed way.

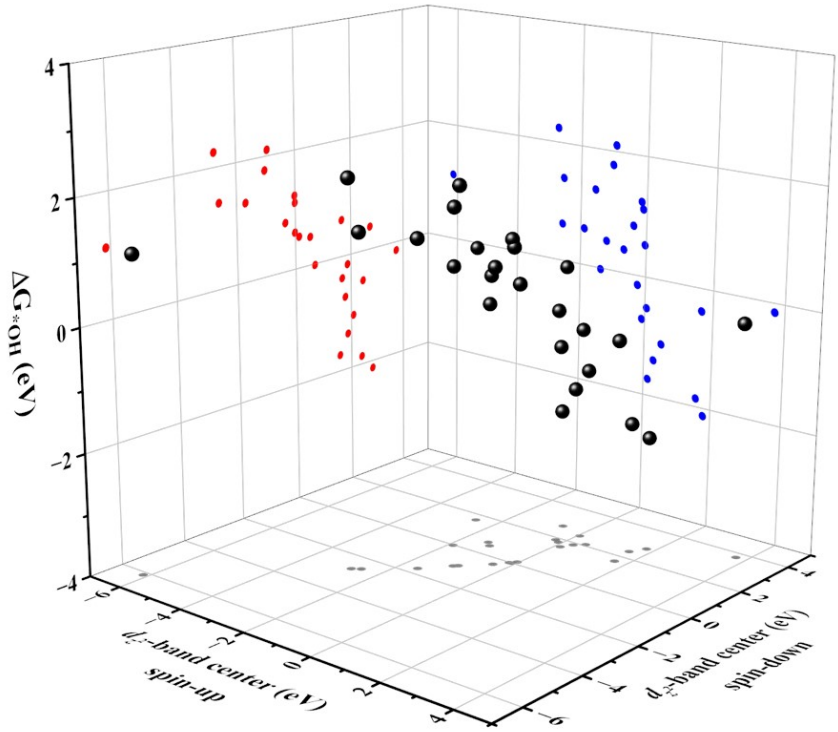

Fig. S10. The variation of ΔG_{*OH} versus spin-polarized d_{z^2}-band centers.

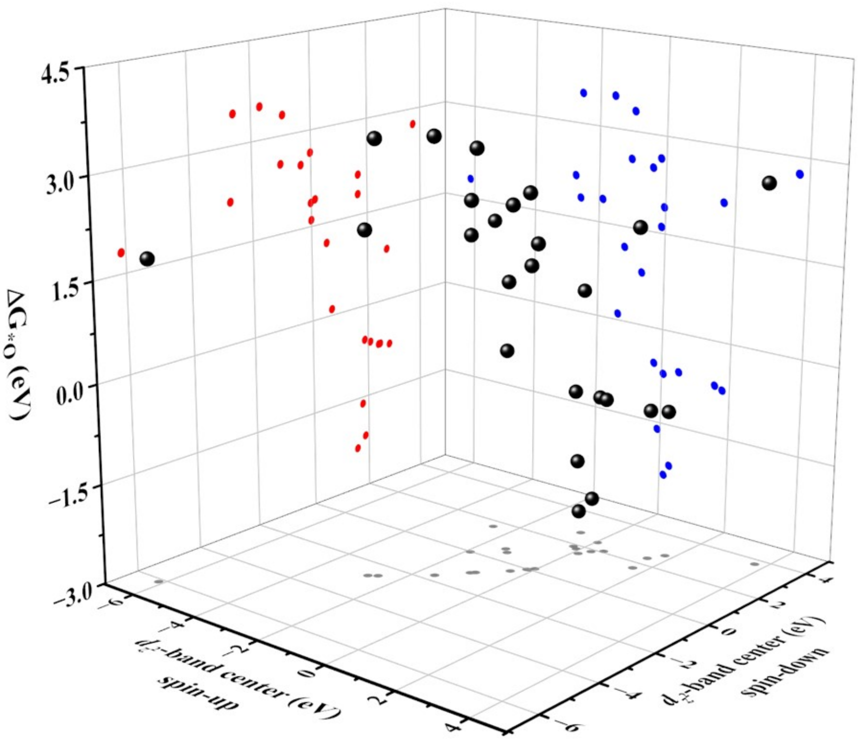

Fig. S11. The variation of ΔG_{*O} versus spin-polarized d_{z^2}-band centers.

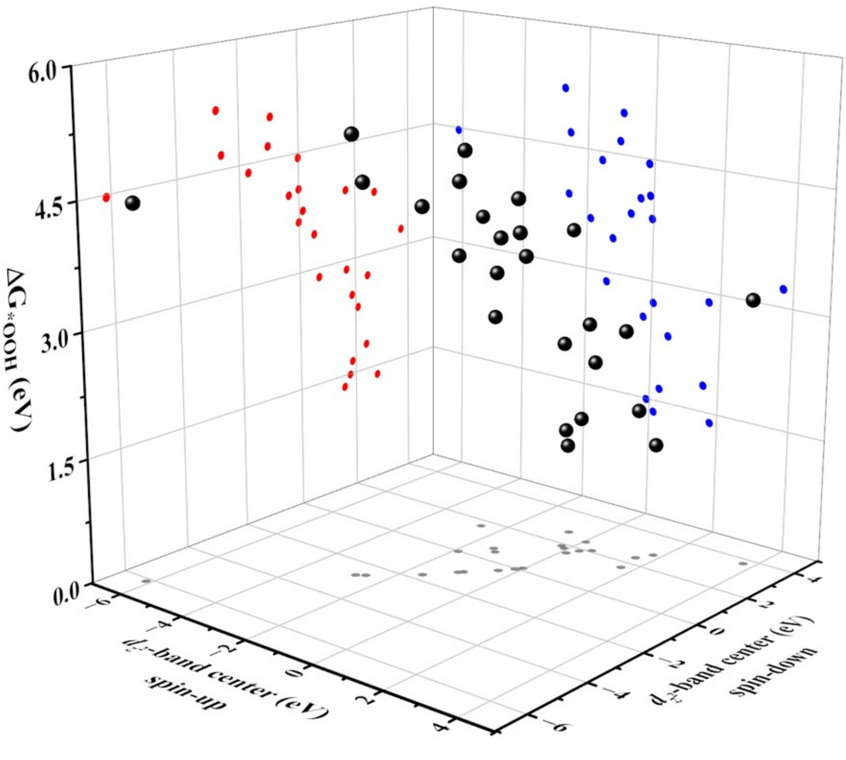

Fig. S12. The variation of ΔG_{*OOH} versus spin-polarized d_{z^2}-band centers.

Table S1. The E_f, Z, U^0_{bulk}, U_{dis} and E_{dis} of TM@g-t-C_4N_3.

TM	E_b (eV)	E_f (eV)	Z*	U^0_{bulk}* (V)	U_{dis} (V)	E_{dis} (V)
Sc	-11.49	-7.37	3	2.46	0.38	0.54
Ti	-10.73	-5.28	2	2.64	1.01	1.25
V	-8.95	-2.92	2	1.46	0.29	0.52
Cr	-8.31	-4.31	2	2.16	1.24	1.48
Mn	-8.99	-5.13	2	2.57	1.38	1.62
Fe	-7.16	-2.29	2	1.15	0.70	0.93
Co	-6.22	-0.95	2	0.48	0.20	0.43
Ni	-6.06	-1.19	2	0.60	0.34	0.57
Cu	-6.46	-2.98	2	1.49	1.64	1.88
Zn	-3.70	-2.58	2	1.29	0.53	0.76
Y	-12.28	-8.15	3	2.72	0.34	0.50
Zr	-12.95	-6.79	4	1.70	0.25	0.37
Nb	-11.55	-4.57	3	1.52	0.42	0.58
Mo	-10.08	-3.87	3	1.29	1.09	1.25
Ru	-7.75	-1.08	3	0.36	0.61	0.77
Rh	-6.87	-1.25	3	0.42	1.17	1.33
Pd	-5.02	-1.31	2	0.66	1.61	1.84
Ag	-3.76	-1.27	1	1.27	2.07	2.54
Hf	-12.93	-6.53	4	1.63	0.08	0.20
Ta	-12.52	-4.25	3	1.42	0.82	0.97
W	-10.39	-1.32	3	0.44	0.54	0.70
Re	-8.56	-0.74	3	0.25	0.55	0.70
Os	-8.19	0.10	8	-0.01	0.83	0.89
Ir	-7.64	-0.32	3	0.11	1.26	1.42
Pt	-6.22	-0.72	2	0.36	1.54	1.78
Au	-3.63	-0.64	1	0.64	2.33	2.80

* data from Ref. 5 for Os and Ref. 6 for others.

The potential of the following reaction (E_{dis}) based on the methods in previous work:[7] TM^{Z+} + Ze^- + g-t-C_4N_3 → TM@g-t-C_4N_3, where Z represents the number of electrons transferred in the reaction. As listed in Table S1. The value of E_{dis} for Ni@g-t-C_4N_3 is 0.57 V, which indicates the Ni@g-t-C_4N_3 might be unstable under the OER/ORR conditions. However, some key factors, for example, the solvent effects, were not considered in our manuscript. Though we found that the solvent effects treated by implicit model have little influence for Gibbs free energy (see Fig. S8), the real effects should be studied more deeply. Therefore, the limitation of our work should be noticed, and simulations under real conditions should be proceeded in future research.

Table S2. The adsorption Gibbs free energies (eV) of *OH, *O and *OOH.

TM	ΔG_{*OH}	ΔG_{*O}	ΔG_{*OOH}	TM	ΔG_{*OH}	ΔG_{*O}	ΔG_{*OOH}
Sc	-0.38	2.14	2.88	**Mo**	-0.16	-0.56	2.53
Ti	-1.08	-0.62	2.35	**Ru**	0.48	1.18	3.44
V	-0.52	-0.70	2.73	**Rh**	1.24	2.65	4.44
Cr	0.39	0.83	3.79	**Pd**	2.10	3.31	5.01
Mn	0.63	1.83	3.90	**Ag**	2.24	2.17	5.21
Fe	0.53	1.91	3.77	**Hf**	-2.13	-0.75	1.38
Co	0.62	1.87	3.64	**Ta**	-1.72	-2.33	--
Ni	0.82	2.49	4.00	**W**	-0.72	-1.61	1.49
Cu	1.31	3.50	4.39	**Re**	-0.02	0.10	2.88
Zn	1.13	1.81	4.47	**Ir**	1.12	1.60	4.05
Y	-0.15	2.75	3.22	**Pt**	1.77	2.57	4.66
Zr	-1.86	-0.70	1.83	**Au**	1.41	3.47	4.67
Nb	-1.38	-2.16	1.66				

Table S3. The energies (eV) of H_2O and H_2 molecules in gas phase.

Molecule	H_2O	H_2
Energy	-14.23	-6.76

Table S4. The reaction Gibbs free energies (eV) in OER and ORR processes. The data marked in blue and red represent the PDSs of OER and ORR, respectively.

TM	ΔG_1	ΔG_2	ΔG_3	ΔG_4	ΔG_5	ΔG_6	ΔG_7	ΔG_8
Sc	-0.38	2.52	0.74	2.04	-2.04	-0.74	-2.52	0.38
Ti	-1.08	0.46	2.97	2.57	-2.57	-2.97	-0.46	1.08
V	-0.52	-0.18	3.43	2.19	-2.19	-3.43	0.18	0.52
Cr	0.39	0.44	2.96	1.13	-1.13	-2.96	-0.44	-0.39
Mn	0.63	1.20	2.07	1.02	-1.02	-2.07	-1.20	-0.63
Fe	0.53	1.38	1.86	1.15	-1.15	-1.86	-1.38	-0.53
Co	0.62	1.25	1.77	1.28	-1.28	-1.77	-1.25	-0.62
Ni	0.82	1.67	1.51	0.92	-0.92	-1.51	-1.67	-0.82
Cu	1.31	2.19	0.89	0.53	-0.53	-0.89	-2.19	-1.31
Zn	1.13	0.68	2.66	0.45	-0.45	-2.66	-0.68	-1.13
Y	-0.15	2.90	0.47	1.7	-1.7	-0.47	-2.90	0.15
Zr	-1.86	1.16	2.53	3.09	-3.09	-2.53	-1.16	1.86
Nb	-1.38	-0.78	3.82	3.26	-3.26	-3.82	0.78	1.38
Mo	-0.16	-0.40	3.09	2.39	-2.39	-3.09	0.40	0.16
Ru	0.48	0.70	2.26	1.48	-1.48	-2.26	-0.70	-0.48
Rh	1.24	1.41	1.79	0.48	-0.48	-1.79	-1.41	-1.24
Pd	2.10	1.21	1.70	-0.09	0.09	-1.70	-1.21	-2.10
Ag	2.24	-0.07	3.04	-0.29	0.29	-3.04	0.07	-2.24
Hf	-2.13	1.38	2.13	3.54	-3.54	-2.13	-1.38	2.13
W	-0.72	-0.89	3.10	3.43	-3.43	-3.10	0.89	0.72
Re	-0.02	0.12	2.78	2.04	-2.04	-2.78	-0.12	0.02
Ir	1.12	0.48	2.45	0.87	-0.87	-2.45	-0.48	-1.12
Pt	1.77	0.80	2.09	0.26	-0.26	-2.09	-0.80	-1.77
Au	1.41	2.06	1.20	0.25	-0.25	-1.20	-2.06	-1.41

Table S5. The overpotentials (V) of OER and ORR for TM@g-t-C_4N_3.

TM	η^{OER}	η^{ORR}
Sc	1.30	1.61
Ti	1.75	2.31
V	2.19	1.75
Cr	1.73	0.84
Mn	0.84	0.60
Fe	0.63	0.70
Co	0.54	0.61
Ni	0.44	0.41
Cu	0.96	0.70
Zn	1.43	0.78
Y	1.67	1.38
Zr	1.86	3.09
Nb	2.58	2.61
Mo	1.85	1.63
Ru	1.03	0.75
Rh	0.56	0.75
Pd	0.87	1.32
Ag	1.81	1.52
Hf	2.31	3.36
Ta	--	--
W	2.20	2.12
Re	1.56	1.25
Ir	1.22	0.74
Pt	0.86	0.97
Au	0.83	0.98

Table S6. The spin-up (UP) and spin-down (DW) projected d-band centers (eV) of anchored TMs.

TM	ε_d		$\varepsilon_{d_{z^2}}$		$\varepsilon_{d_{xz}}$		$\varepsilon_{d_{yz}}$		$\varepsilon_{d_{xy}}$		$\varepsilon_{d_{x^2-y^2}}$	
	UP	DW	UP	DW	UP	DW	UP	DW	UP	DW	UP	DW
Sc	1.72	1.72	1.67	1.67	1.52	1.49	1.50	1.49	2.06	2.06	2.05	2.06
Ti	0.74	1.57	0.51	2.08	0.77	1.53	0.77	1.53	0.90	1.43	0.89	1.43
V	-0.08	1.85	0.05	2.45	-0.11	1.92	-0.19	2.19	-0.04	1.42	-0.01	1.46
Cr	-0.90	2.17	-0.67	2.72	-0.99	2.42	-1.01	2.42	-0.89	1.70	-0.89	1.71
Mn	-2.42	1.66	-2.57	1.66	-2.63	1.58	-2.65	1.57	-2.12	1.77	-2.11	1.78
Fe	-0.45	-0.32	-0.04	0.13	-0.62	0.14	-0.45	-0.07	-0.65	-0.73	-0.43	-0.97
Co	-2.45	0.02	-1.89	-0.02	-2.42	0.23	-2.27	0.06	-2.88	-0.15	-2.88	-0.06
Ni	-1.05	-0.99	-0.39	-0.35	-0.68	-0.64	-0.83	-0.79	-1.54	-1.45	-1.61	-1.52
Cu	-1.71	-1.94	-1.56	-1.7	-1.66	-1.83	-1.78	-1.94	-1.68	-2.08	-1.83	-2.08
Zn	-6.09	-6.08	-6.14	-6.14	-6.15	-6.14	-6.27	-6.26	-5.94	-5.93	-5.91	-5.90
Y	3.89	3.87	3.72	3.73	3.34	3.36	3.33	3.36	4.34	4.37	4.35	4.35
Zr	1.84	2.18	1.57	2.39	1.42	1.70	1.42	1.69	2.48	2.64	2.48	2.64
Nb	0.45	1.35	0.29	1.87	0.04	0.99	0.03	1.00	1.00	1.53	1.00	1.53
Mo	-0.47	1.34	-0.24	1.87	-0.80	1.52	-0.80	1.52	-0.19	1.04	-0.19	1.03
Ru	-1.39	-0.47	-1.20	0.52	-1.30	-0.54	-1.29	-0.54	-1.49	-0.80	-1.50	-0.80
Rh	-0.93	-0.71	-0.16	-0.02	-0.75	-0.47	-0.74	-0.47	-1.41	-1.21	-1.41	-1.21
Pd	-1.45	-1.46	-0.95	-0.95	-1.33	-1.32	-1.32	-1.32	-1.79	-1.80	-1.79	-1.80
Ag	-2.85	-2.84	-2.73	-2.72	-2.91	-2.90	-2.91	-2.90	-2.82	-2.81	-2.82	-2.81
Hf	2.12	2.48	1.79	2.80	1.84	2.19	1.85	2.19	2.72	2.79	2.72	2.80
Ta	0.29	0.97	0.13	1.57	0.08	0.82	0.09	0.81	0.80	1.05	0.80	1.06
W	-0.28	1.23	-0.09	1.78	-0.66	1.37	-0.66	1.36	0.15	1.01	0.15	1.02
Re	-1.54	-0.01	-1.37	0.68	-1.89	-0.03	-1.89	-0.02	-1.15	-0.19	-1.15	-0.20
Ir	-1.01	-0.84	-0.11	-0.01	-0.83	-0.61	-0.84	-0.61	-1.51	-1.37	-1.51	-1.37
Pt	-1.68	-1.69	-1.03	-1.04	-1.55	-1.56	-1.56	-1.56	-2.05	-2.07	-2.06	-2.07
Au	-2.77	-2.84	-2.54	-2.58	-2.86	-2.88	-2.86	-2.88	-2.80	-2.92	-2.81	-2.92

Table S7. The linear relationship between projected band centers of d_{xz}, d_{yz}, d_{xy}, $d_{x^2-y^2}$, group d_{xz}-d_{yz}, group d_{xy}-$d_{x^2-y^2}$ and d_{z^2}-band center in spin-up (UP) and spin-down (DW) channels.

orbitals (UP)	**Linear equation**	**R²**	**orbitals (DW)**	**Linear equation**	**R²**
d_{xz}	$\varepsilon_{d_{xz}} = 0.99\varepsilon_{d_{z^2}} - 0.29$	0.98	d_{xz}	$\varepsilon_{d_{xz}} = 0.95\varepsilon_{d_{z^2}} - 0.38$	0.98
d_{yz}	$\varepsilon_{d_{yz}} = 1.00\varepsilon_{d_{z^2}} - 0.30$	0.99	d_{yz}	$\varepsilon_{d_{yz}} = 0.96\varepsilon_{d_{z^2}} - 0.40$	0.99
d_{xy}	$\varepsilon_{d_{xy}} = 1.10\varepsilon_{d_{z^2}} - 0.05$	0.91	d_{xy}	$\varepsilon_{d_{xy}} = 1.01\varepsilon_{d_{z^2}} - 0.53$	0.94
$d_{x^2-y^2}$	$\varepsilon_{d_{x^2-y^2}} = 1.10\varepsilon_{d_{z^2}} - 0.04$	0.91	$d_{x^2-y^2}$	$\varepsilon_{d_{x^2-y^2}} = 1.01\varepsilon_{d_{z^2}} - 0.53$	0.93
d_{xz} **&** d_{yz}	$\varepsilon_{d_1} = 1.00\varepsilon_{d_{z^2}} - 0.29$	0.98	d_{xz} **&** d_{yz}	$\varepsilon_{d_1} = 0.95\varepsilon_{d_{z^2}} - 0.39$	0.98
d_{xy} **&** $d_{x^2-y^2}$	$\varepsilon_{d_2} = 1.10\varepsilon_{d_{z^2}} - 0.05$	0.91	d_{xy} **&** $d_{x^2-y^2}$	$\varepsilon_{d_2} = 1.00\varepsilon_{d_{z^2}} - 0.53$	0.94

References

1. X. Chen, Q. Liu, H. Zhang and X. Zhao, Exploring high-efficiency electrocatalysts of metal-doped two-dimensional C_4N for oxygen reduction, oxygen evolution, and hydrogen evolution reactions by first-principles screening, *Phys. Chem. Chem. Phys.*, 2022, **24**, 26061-26069.
2. G. V. Gibbs, D. F. Cox, N. L. Ross, T. D. Crawford, R. T. Downs and J. B. Burt, Comparison of the electron localization function and deformation electron density maps for selected earth materials, *J. Phys. Chem. A*, 2005, **109**, 10022-10027.
3. S. Dong, C. Li, E. Lv, J. Wang, H. Liu, Z. Gao, W. Xiong, Z. Ding, W. Yang and H. Li, MgH_2/single-atom heterojunctions: effective hydrogen storage materials with facile dehydrogenation, *J. Mater. Chem. A*, 2022, **10**, 19839-19851.
4. C.-S. Yin, Y. Leng, X. Yang, C.-G. Min, A.-M. Ren, Unraveling the mechanism of pyrrole and N-defect regulating CoN_4 single atom catalysts as a pH-universal bifunctional electrocatalyst for OER and ORR, *Appl. Surf. Sci.*, 2024, **643**, 158605.
5. X. Guo, J. Gu, S. Lin, S. Zhang, Z. Chen, S. Huang, Tackling the Activity and Selectivity Challenges of Electro-catalysts toward the Nitrogen Reduction Reaction via Atomically Dispersed Biatom Catalysts, *J. Am. Chem. Soc.* 2020, **142**, 5709–5721.
6. David R. Lide, ed., CRC Handbook of Chemistry and Physics, Internet Version 2005, <http://www.hbcpnetbase.com>, CRC Press, Boca Raton, FL, 2005.
7. A. S. Dobrota, N. V. Skorodumova, S. V. Mentus, I. A. Pašti, Surface pourbaix plots of M@N4-graphene single-atom electrocatalysts from density functional theory thermodynamic modeling, *Electrochimica Acta* 2022, **412**, 140155.